Architectures and dynamics of a late Quaternary coarse-grained barrier complex at the inlet of a hypertidal estuary (South Patagonia, Argentina)

Léo Pancrazzi, Bernadette Tessier, Pierre Weill, Dominique Mouazé, José Ignacio Cuitiño, Jean-Yves Reynaud, Maria Duperron, Roberto Adrián Scasso, Alejandro Montes

Journal of South American Earth Sciences 146 (2024) 105073

Contents lists available at ScienceDirect

Journal of South American Earth Sciences

journal homepage: www.elsevier.com/locate/jsames

Architectures and dynamics of a late Quaternary coarse-grained barrier complex at the inlet of a hypertidal estuary (South Patagonia, Argentina)

Léo Pancrazzi [a,b,*], Bernadette Tessier [a], Pierre Weill [a], Dominique Mouazé [a], José Ignacio Cuitiño [c], Jean-Yves Reynaud [d], Maria Duperron [e], Roberto Adrián Scasso [e], Alejandro Montes [f,g]

[a] Université de Caen Normandie, CNRS, Univ Rouen Normandie, Normandie Univ, UMR 6143 M2C, 14000, Caen, France
[b] Department of Geography, UCL, Gower Street, London, WC1E 6BT, UK
[c] Instituto Patagónico de Geología y Paleontología, CCT CONICET-CENPAT, Boulevard Almirante Brown 2915, U9120CD, Puerto Madryn, Chubut, Argentina
[d] UMR 8187, LOG, Laboratoire d'Océanologie et de Géosciences, Univ. Lille, CNRS, Univ. Littoral Côte d'Opale, F-59000, Lille, France
[e] Instituto de Geociencias Básicas, Aplicadas y Ambientales de Buenos Aires (IGeBA), Departamento de Ciencias Geológicas, Facultad de Ciencias Exactas y Naturales, Universidad de Buenos Aires-CONICET, Ciudad Universitaria, Pabellón II, Buenos Aires, C1428, Argentina
[f] Centro Austral de Investigaciones Científicas (CADIC-CONICET), B. Houssay 200, Ushuaia, 9410, Argentina
[g] Universidad Nacional de Tierra del Fuego, Antártida e Islas del Atlántico Sur, Fuegia Basket 251, 9410, Ushuaia, Tierra del Fuego, Argentina

ARTICLE INFO

Keywords:
Gravel barrier
Ground-penetrating radar
Hypertidal
Sea level change
Patagonia

ABSTRACT

The southern coast of Argentina is known for its high tidal ranges and large coarse-grained coastal barriers that have emerged over time as a result of the regional uplift. Well-preserved barriers can provide critical information about the morphological evolution of the coastal areas, and the relative evolution of the mean sea level, as long as their morphodynamics are well understood. In order to better understand the influence of tides in wave-built sedimentary bodies, an in-depth analysis of the architecture of a barrier system has been realized at the mouth of the Santa Cruz - Chico river estuary (50°S). Maximum tidal range in this estuary is 12 m. A great variety of morphologies compose both sides of the estuary inlet, from simple ridges and barrier spits to beach ridge plains. Barrier spits and beach ridge plains characterize the southern side, whereas elongated simple ridges and barrier spits isolating large tidal flats are more developed on the northern side. The site was investigated using ground-penetrating radar combined with digital elevation model analysis, and some sedimentological observations. Cross-shore profiles, with a penetration depth up to 5 m, show a large range of radar facies attributed to erosional surfaces, beach face progradation, and washover deposits. The slope of the beach face appears to be an effective parameter for differentiating between beach ridges plains and barrier spits, as the latter are characterized by steeper values. The combined analysis of the radar architecture and barrier morphology allows to identify five barrier sets, which have been associated with five different development stages along the late Quaternary: 1) Last Interglacial Maximum (MIS 5e), 2) Last Interglacial (MIS 5e/5c/5a), 3) Mid Holocene transgressive maximum, 4) Mid Holocene highstand reworking, and 5) Holocene regressive stage. Although the morphological model is in line with the observations made by other authors, it would be appropriate to consolidate the model by establishing an absolute chronology.

1. Introduction

The Atlantic coast of Patagonia (40–55°S) and its numerous coarse-grained coastal barriers have been shaped during the late Quaternary in a complex environment governed by tectonic uplift, global sea-level changes, and tidal range variations along the coast from 1 to 10 m (Codignotto et al., 1992; Isla and Bujalesky, 1995; Schellmann and Radtke, 2000, 2003, 2010). A number of studies address the relative sea-level variations in this region through the study of morphological features such as marine terraces (e.g., Feruglio, 1950; Codignotto et al., 1988; Rostami et al., 2000; Pedoja et al., 2011) and coastal barriers (e.g., Codignotto et al., 1990; Schellmann, 1998; Schellmann and Radtke, 2000, 2003, 2010; Isla and Bujalesky, 2008; Zanchetta et al., 2014; Pappalardo et al., 2015). The use of coastal barrier morphology and

* Corresponding author. Université de Caen Normandie, CNRS, Univ Rouen Normandie, Normandie Univ, UMR 6143 M2C, 14000, Caen, France.
E-mail address: l.pancrazzi@ucl.ac.uk (L. Pancrazzi).

https://doi.org/10.1016/j.jsames.2024.105073
Received 11 June 2024; Received in revised form 4 August 2024; Accepted 5 August 2024
Available online 8 August 2024

architecture as a relative sea-level marker is not as reliable as the use of marine terraces, but it has the advantage of providing higher resolution information at the Holocene scale (e.g., Billy et al., 2015; Nielsen et al., 2017; Brooke et al., 2019). Despite the control of extreme events on coastal barrier morphology (Orford and Anthony, 2011), the use of gravel ridge height for relative sea-level estimation can be reliable, especially in isostatically-uplifted coasts (Sanjaume and Tolgensbakk, 2009; Tamura, 2012), and in wave-protected environments like estuaries (Orford et al., 1991; Schellmann and Radtke, 2010). According to reviews such as those of Otvos (2000) and Tamura (2012), the use of prograded beach deposits for paleoenvironmental reconstructions must be carried out with care and requires a good knowledge of their specific morphodynamics.

The morphodynamics of coastal barriers in estuarine environments, especially when the latter experience significant tidal ranges, is far from obvious for several reasons: (1) the complexity of hydrodynamics combining wave action, tidal processes and fluvial dynamics (Dalrymple et al., 2012), (2) the great diversity of estuarine morphologies where barriers can develop and consequently the great diversity of coast exposure relative to main wave directions, and (3) the convergence of sediment fluxes that interact with each other (Elias and Hansen, 2013). Some examples along the English Channel coasts, mostly sandy systems, have demonstrated the power of tidal processes to modify the rate of development of sedimentary bodies (Levoy et al., 2000; Robin et al., 2009; Montreuil et al., 2014), but also the potential of preservation of these processes within the internal architecture of sandy and coarse-grained barrier spits (Fruergaard et al., 2020; Pancrazzi et al., 2022). Observations are still scattered and need to be confirmed with other case studies.

Several studies have been carried out to understand the morphodynamics of coastal barriers along the Patagonian coast (e.g. Kokot, 1999; Iantanos, 2004; Kokot et al., 2005; Ercolano, 2010; Kokot, 2010; Isla and Bujalesky, 2000, 2008; Bujalesky, 2007). The majority of the literature highlights how gravel systems organise themselves at the inlet of ria-type estuaries. The high tidal ranges generated in this environments, combined with varying exposures to Atlantic waves, enhance and control the deposition of fine sediments (Isla et al., 2004), which in turn influence the development of gravel barriers. However, studies on the internal architecture of these systems are relatively sparse (Montes et al., 2018; Nunes et al., 2023). This study aims to provide stratigraphic and morphological description of a coarse-grained coastal barrier system, composed of several barrier types, located in a mixed-energy tidal inlet. The studied system is located at the mouth of the Santa-Cruz – Chico river estuary, in South Patagonia (Santa Cruz Province, Argentina). The present study is part of a larger project the objective of which was to explore the morphodynamic behavior and Holocene sediment infill stratigraphy of this giant hypertidal estuary (Tessier et al., 2024). A combination of ground-penetrating radar (GPR) data, elevation data from digital elevation model (DEM), and field observations is used to (1) better understand the morphodynamics of coarse-grained barriers in mixed-energy environments, (2) reconstruct the morphological evolution of the barrier system during the late Quaternary, and (3) provide further information on the evolution of the relative sea-level changes in Southern Patagonia.

2. Study area

The Santa Cruz – Chico river (SCCR) estuary is located in the Province of Santa Cruz, a semi-arid region in the southern coast of Argentina (50° S). This area is a passive margin where uplift rates have been estimated to 0.11 ± 0.03 mm/yr since the Last Interglacial Maximum (Pedoja et al., 2011). As all the Patagonian estuaries, the Santa Cruz – Chico river estuary is a drowned valley, incised into the Miocene sedimentary rocks of the Monte León Formation that forms part of the Austral basin infilling (Piccolo and Perillo, 1999). The estuary is composed of an approximately 25 km-long and 5 km-wide basin with a NW-SE orientation open to the South Atlantic Ocean through a 2 km wide inlet. Two rivers converge at the head of this estuary, the Santa Cruz river from the south-west and the Chico river from the north-west (Fig. 1A). The southern bank of the estuary is characterized by 120 m-high cliffs mainly formed by the Monte León Formation, made of sandstones, mudstones and tuffs (Bertels, 1970; Parras and Griffin, 2009). The northern bank has a much gentler profile and is characterized by extensive fluvial terraces which include 6-10 m-thick layers of gravel known locally as '*Rodados Patagonicos*' (Darwin, 1846). Coarse-grained barriers are located on both sides of the estuary, shaping the narrow inlet (Fig. 1B).

The SCCR estuary experiences semi-diurnal tides and a hypertidal range (*sensu* Archer, 2013), reaching up to 12 m during highest spring tides (Servicio de Hidrografía Naval, Argentina). The highest tidal currents occur at the mouth of the estuary, with velocities of 3–4 m s^{-1} (Bindelli et al., 2020). The mean annual discharges of the Santa Cruz and the Chico rivers are about 715 m^3 s^{-1} and 25 m^3 s^{-1}, respectively (Bindelli et al., 2020). Exceptional river floods occur, frequently in March, due to ice dam collapse in the Perito Moreno glacier area, further upstream in the headwaters of the Santa Cruz river (Pasquini and Depetris, 2011). Daily discharge of the Santa Cruz river can then reach up to 2500 m^3 s^{-1} (Piccolo and Perillo, 1999). Nevertheless, water level beyond the confluence of both rivers is not influenced by the river discharge (Ezcurra and Schmidt, 2017). Dominant winds blow from the west and can reach velocities up to 100 or exceptionally up to 200 km h^{-1} (Piccolo and Perillo, 1999). Mean significant wave height in front of the inlet, based on a global ocean physics reanalysis between 2010 and 2020 (data source: Copernicus Marine Data Store), ranges from 0.5 to 1 m without major differences between seasons. The wave directions are homogeneously distributed from the north-east to the south-west with a small dissymmetry to the south-west. The short-period swells (less than 9 s) from south-west to south directions represent 22% of the sea state and mainly occur during the austral summer. The highest waves are generated during the summer period, where 3% of the wave heights ranges between 2 and 3 m, reaching occasionally maximum heights of 4.5 m. The longest swells have periods ranging from 10 to 17 s with directions from north-east to south-east, representing 13% of the sea state. The wave height of these long swells usually remains below 1 m.

3. Methodology

The morphological and sedimentological characterization of the mouth of the SCCR estuary has been performed using field observations, a satellite image (Google Earth) and a digital elevation model (DEM) from 2015 (5 m horizontal resolution) (IGN, Instituto Geográfico Nacional de la República Argentina). Both the satellite image and DEM have been analysed with QGIS 3.4 (QGIS Development Team, 2018) to identify, delimit and digitise the different ridges and barrier units.

A ground-penetrating radar (GPR) investigation was performed using two GPR systems from GSSI (Geophysical Survey Systems, Inc.; Nashua, New Hampshire, USA): (1) GPR SIR-3000 system with a 400 MHz shielded antenna, and (2) GPR SIR-4000 system with a 350 MHz HS digital antenna. A total of 21,7 km of GPR data, distributed over 95 lines, have been collected during two fields campaigns in December 2019 and February 2023. The GPR lines were positioned either perpendicular or parallel to the barrier ridges (Figs. 2 and 3). A basic data processing was performed with the GPRPy software (Plattner, 2020), which includes time-zero adjustment, dewow, background removal, time-depth conversion, migration (f-k Stolt), and topographic correction. The velocity of wave propagation is calculated by analysing the reflection hyperbolas for each area (Bristow and Jol, 2003), and the values vary between 0.1 and 0.15 m ns^{-1}. These values remain consistent with the velocity range in unsaturated sand and gravel deposits (Neal and Roberts, 2000). The topographic data from the DEM was used to perform the topographic correction. Given the low amplitude and large wavelength of the terrain irregularities, the 5-m resolution of the DEM was adequate to achieve

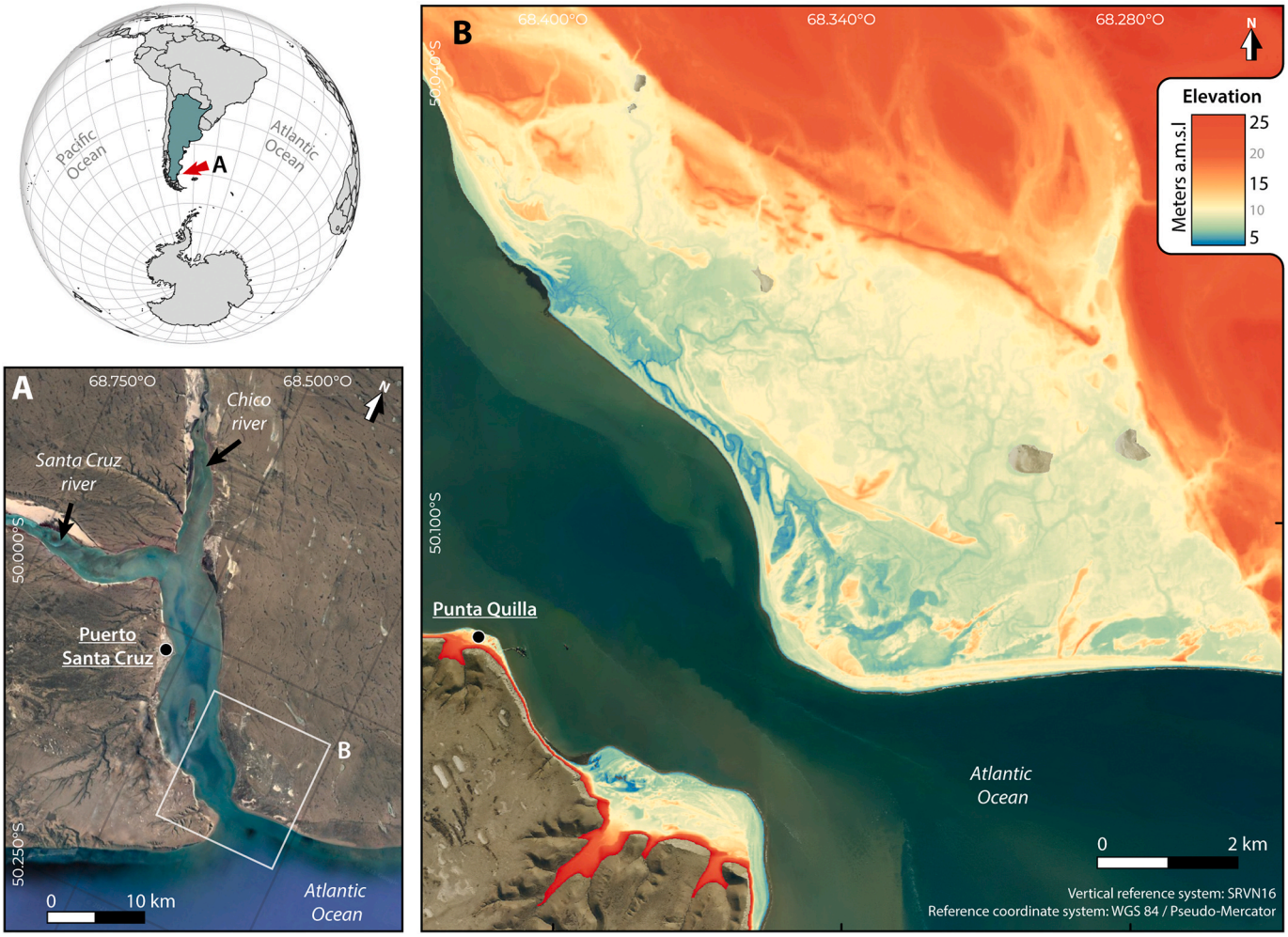

Fig. 1. Location of the Santa Cruz – Chico river estuary. (A) Google Earth view of the SCCR estuary, (B) Digital elevation model of the inlet of the SCCR estuary (IGN, Insituto Geográfico Nacional de la República Argentina).

coherent correction.

4. Results

4.1. Barrier system description: barrier types and distribution

The DEM clearly shows highly asymmetric morphology and extension of the barrier system at both sides of the inlet (Fig. 1). DEM analysis allows delineating different barrier sets on the basis of their elevation: five in the north (N1-N5) and two in the south (SI-S2) (Fig. 2). Three main barrier types are identified: simple ridges (composed of a single ridge, the end of which can be recurved), barrier spits (elongated barriers composed of one or more ridges with several recurved endings), and beach ridge plains (composed of a series of linear and parallel ridges). To simplify the morphological description, when spits or barriers show a direction of elongation towards the sea, i.e. they are getting out from the estuary, it is defined as seaward elongation. On the contrary when spits and barriers elongate towards the head of the estuary, i.e. they are getting into the estuary, the elongation is defined as landward.

4.1.1. Northern area

The coarse-grained barrier system on the northern bank of the inlet is located over a large, and for the most part inactive, tidal flat, covering an area of approximately 45 km^2. This tidal flat is presently highly vegetated and drained by a complex network of channels (Figs. 2 and 3A). The elevation of the tidal flat ranges from 7 to 8 m above mean sea level (a.m.s.l.) (Fig. 1B). According to elevation, as well as morphology and location, barriers were grouped into 5 distinct sets (N1-N5):

- N1: a barrier set ranging from 13.5 to 16.5 m a.m.s.l., located along the northern edge of the tidal flat, in contact with the lowest fluvial terrace (N1a - Fig. 2). Barriers within the set are elongated shore-parallel gravel ridges, displaying a fine silt-dominant matrix visible on the ground surface. The lowest barriers of this set are more discontinuous (N1b – Fig. 2), due to the presence of fluvial and tidal (paleo) channels that dissect the ridges.
- N2: a barrier set ranging from 11 to 14.5 m a.m.s.l. Situated in various areas and characterized by different elongation directions. To the East, barriers are characterized by recurved morphologies pointing N-NE, i.e. perpendicular to the present coastline (N2a – Fig. 2). In the central part, only the end section of a recurved spit featuring a seaward elongation is preserved (N2b – Fig. 2). In the westernmost part, the main barrier of the set is composed of several parallel ridges, the termination of which features a seaward elongation (N2c – Fig. 2). A secondary barrier, composed by several recurved ridges elongating landward, is situated in the prolongation of the main barrier (N2d – Fig. 2). All barriers of this set, except the main one (N2c), display a fine silt-dominant matrix on their surface.
- N3: a set ranging from 10.5 to 12 m a.m.s.l. and composed of two main barrier units (N3a and N3b). The first unit, which is situated approximately in the centre of the tidal flat (N3a – Fig. 2), obliquely overlaps a barrier unit from the previous set (N2b). This barrier unit

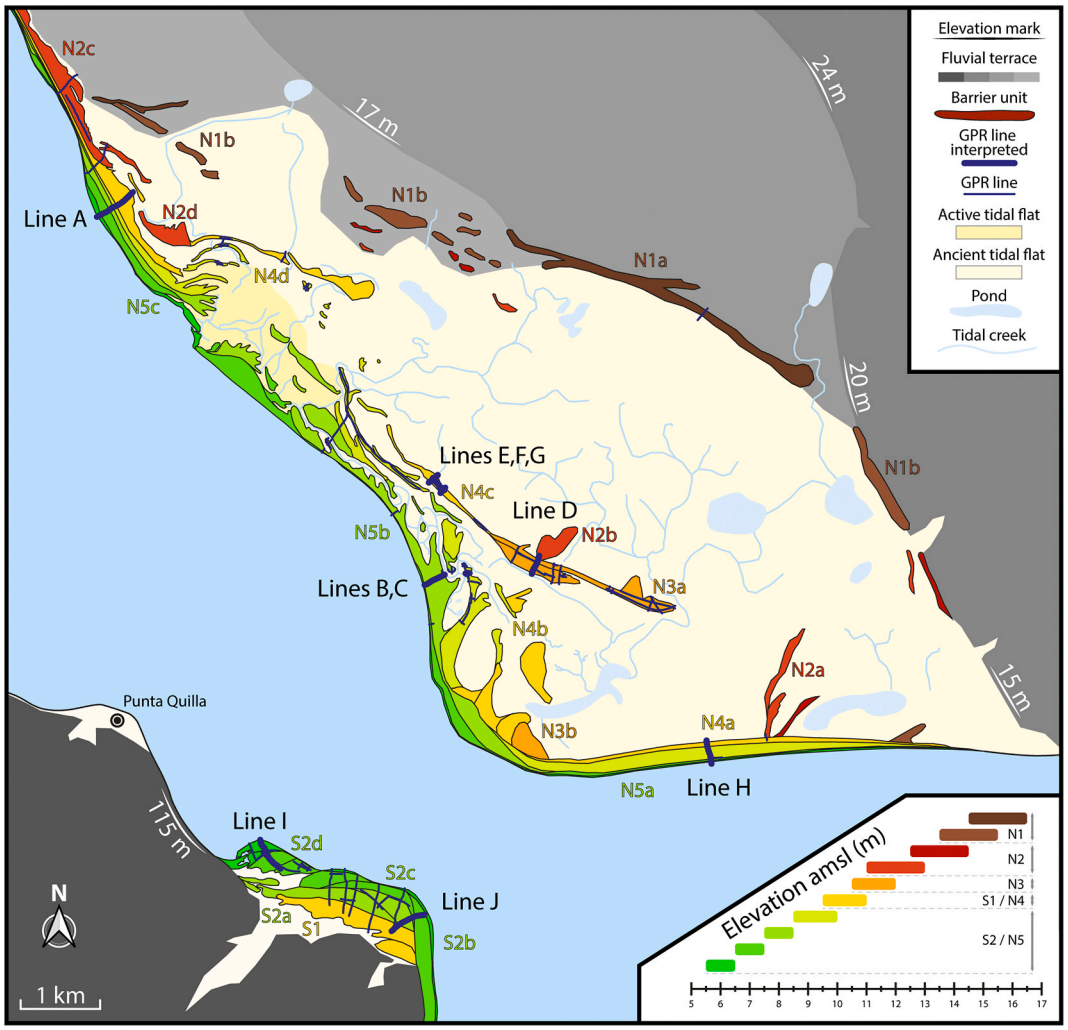

Fig. 2. Morphological map of the coastal barrier systems of the SCCR estuary and location of the GPR profiles. Barrier sets situated at elevation ranging from 5.5 to 16.5 m are illustrated by different colours.

which extends over 2.5 km is composed of several parallel ridges oriented NW-SE (Fig. 3B) with spit terminations on the eastern part, i.e. featuring a seaward elongation. The second barrier unit of this set is situated 1.5 km south of the first one, close the current inlet (N3b – Fig. 2). Only the hook terminations of this unit seem to be preserved, and indicate a spit elongation landward.

- N4: a set ranging from 9.5 to 11 m a.m.s.l., situated on the seaward edge of the tidal flat, and parallel to the present-day coastline. To the East, a longitudinal barrier intersects the unit N2a. Hooked spits, entering into the estuary, characterize the terminations of this barrier unit at the inlet (N4b – Figs. 2 and 3C). The barrier units situated on the central area correspond to narrow and longitudinal ridges oriented NW-SE (N4c – Fig. 2). To the West, barrier units correspond to barrier spits with multiple hook terminations pointing to SE, i.e. seaward (N4d – Fig. 2). The direction of these barriers is the same as N2c.
- N5: a set ranging from 5.5 to 10 m a.m.s.l. that forms the current coastline morphology. N5a is a beach ridge unit, parallel to N4a and connected to N5b (Fig. 2). The ridges of this set, mainly represented by the unit N5b have terminations that indicate a landward elongation (N5b – Figs. 2 and 3C). N5c is a barrier spit unit parallel to N2c and N4d and have the same direction, i.e. featuring a seaward elongation (N5c – Fig. 2). The units N5b and N5c almost entirely isolate the tidal flat, the only remaining opening being located at the junction between these two units. The active beach is composed by berms in the steep upper foreshore zone composed of pebbles, and a mid- and low-tide zone composed of fine sands and a gentle gradient (Fig. 3D).

4.1.2. *Southern area*

The barrier system on the southern bank encompasses an area of approximately 2 km^2 that has formed at the outlet of a valley (100 m deep, 800 m wide) that incises the Miocene Monte León Formation (Fig. 1B). The system comprises barrier spits and beach ridges, oriented globally E-W and N-S. Two distinct barrier sets, ranging in elevation from 5.5 to 11 m, have been identified (S1-S2):

- S1: a set ranging from 9.5 to 11 m a.m.s.l., situated on the southern edge of the system, in contact with the foot of the Miocene cliff (Fig. 4A). It is mainly composed of a single 2 km-long barrier spit unit displaying some hook terminations featuring a westward (i.e. landward) elongation. The surface of the barriers is highly vegetated with mainly low vegetation (grass and bushes).
- S2: a set ranging from 5.5 to 8.5 m a.m.s.l. which can be divided in two groups. The most elevated units of the sets, ranging from 7.5 to 8.5 m are beach ridges around 300 m wide, developing toward the north and then toward the east (S2a – Fig. 2). The western termination of this group almost completely blocks the flow of the stream coming from the valley. The vegetation is characterized by small trees that grow preferentially on the crest of the gravel ridges. The

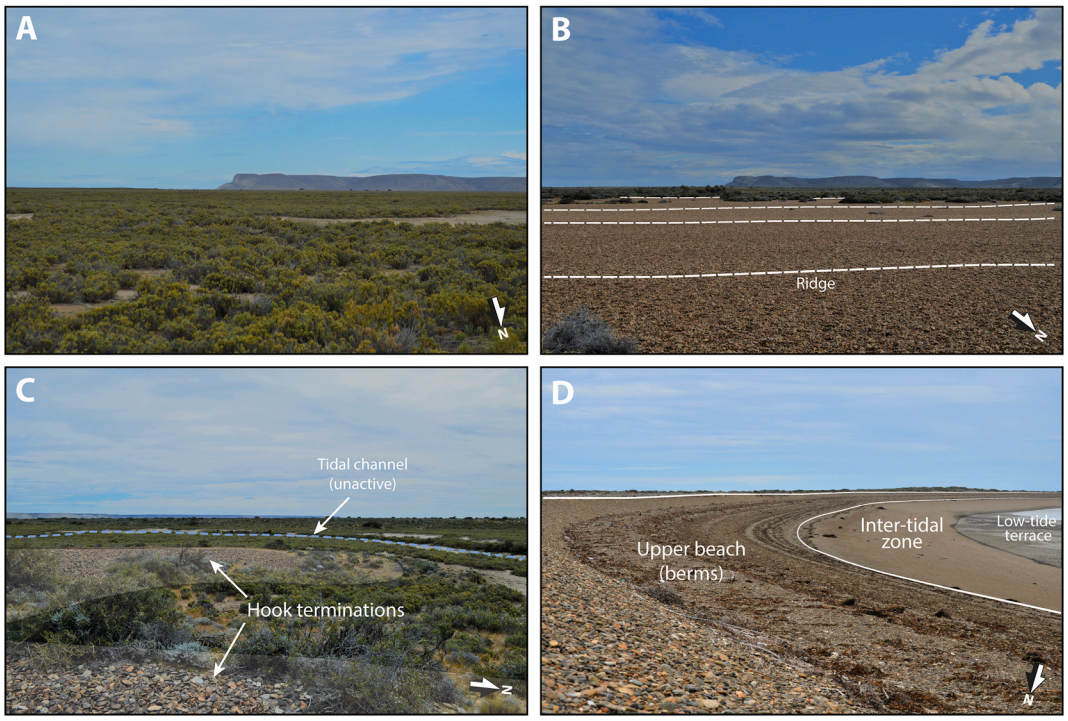

Fig. 3. Field photographs of the northern area of the SCCR estuary inlet: (A) Tidal flat, (B) Top of the barrier spit unit N3a, (C) Hook termination of a barrier spit unit in N5, (D) Active beach profile inside the estuary.

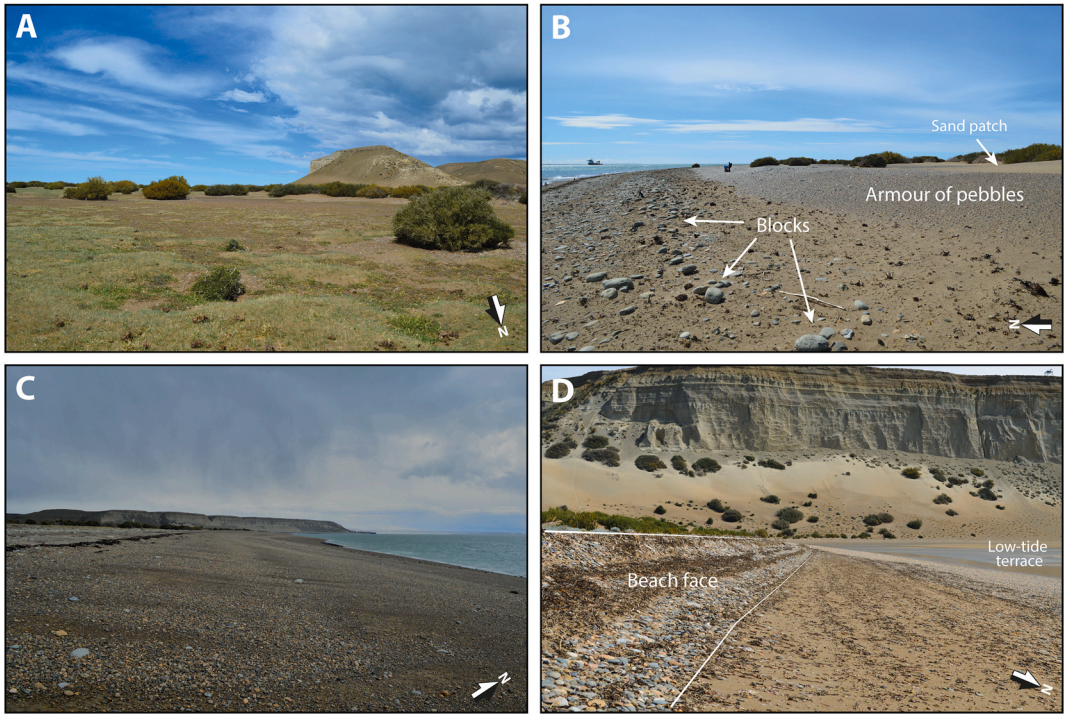

Fig. 4. Field photographs of the southern area: (A) Vegetation on the barrier (S1) and paleocliff behind, (B) Surface sedimentological variability on the foreshore (S2c), (C) Active beach profile of the beach ridge unit S2c composed of mixed sand-and-gravel sediments, (D) Sediment sorting in the active beach profile of the barrier spit units S2d.

lowest units of the set, ranging from 5.5 to 7.5 m, form the current coastline morphology and are composed of different barrier morphologies depending on their position. To the east, the set is characterized by beach ridges units oriented N-S with an average width of 250 m (S2b – Fig. 2). In the eastern part, the set cuts obliquely the older ones oriented ENE-WSW, while in the north the set is parallel to the previous set (S2c – Fig. 2). There is still vegetation on the most landward units but it progressively disappears towards the sea. The surface of the western beach ridge units is characterized by an armour of pebbles of about 5–10 cm in diameter over which there are

some æolian sand patches (Fig. 4B). On the eastern side, blocks of a few decimetres, underline the ridge crests. The active beach profile of the beach ridge units is composed of mixed sand and gravel sediments, except for the bottom of the profile which is mainly composed of coarse-grained sediment (Fig. 4C). To the west, the set is composed of barrier spit units displaying an upstream part with signs of erosion, and well-preserved hook terminations recurved towards the SW (S2d – Fig. 2). The surface of these western barrier units is covered by an aeolian sand layer and bushes. The active beach profile of the barrier spit units is characterized by a narrow and steep coarse-grained upper part, a mixed sand-and-gravel intermediate part, and a large tidal flat in the lower part over which swash bars migrate onshore (Fig. 4D). The barrier spit units S2a and S2d are crossed by a tidal channel which is connected to the outlet of the valley system.

4.2. Sedimentary architecture of the coarse-grained barriers

Ten GPR lines, distinguished from A to J, have been selected to describe the sedimentary architecture of the different barrier morphologies located at different elevations at the mouth of the SCCR estuary. All GPR lines, except line E, are perpendicular to the ridges.

4.2.1. Line A

GPR line A is a 550 m-long cross-shore profile, oriented SW-NE, located over barrier spit units from set N4 and N5, whose elevations range from 6 to 10 m (Figs. 2 and 5). The average signal penetration depth is 2 m, decreasing progressively seaward to about 1 m. Line A is characterized by seaward-dipping reflections with slopes ranging from 5 to 13.5°. According to their elevation, these reflections correspond to beach face geometries. In the first 300 m of the line, where the barrier elevation increases from 6 to 10 m, the slope of the beach face decreases progressively from 10 to 7°. The maximum slope values are found at the boundaries of each set, where the change in elevation occurs. Between 300 and 550 m, the elevation of the barrier is stabilized between 9 and 10 m and the inclination of the reflections is between 9.5 and 12.5°. The most landward section of the line is characterized by three high-amplitude concave reflections whose inclination decreases from 11 to 5.5°. The last few dozen meters show a chaotic facies with highly heterogeneous reflections.

4.2.2. Lines B-C-D

GRP lines B, C and D are situated within a cross-shore section in the central part of the northern area cutting three barrier sets (N2, N3 and N5) and oriented NE-SW. The section starts on an active barrier unit at an elevation of 7 m and ends on an older barrier unit with an elevation of 12 m (Fig. 6d). Lines B and C correspond each to a single barrier set, line D encompasses two barrier sets. The barrier morphologies described with these three GPR lines are three kinds of barrier spits separated from each other by an area of highly-vegetated tidal flat.

Line B is a 325 m-long profile that crosses a barrier spit to a beach ridge unit elongated towards the north with an elevation between 7 and 8 m that belongs to set N5. (Fig. 6a). The mean signal penetration depth is 2 m in the first 50 m, increases to 5 m between 50 and 315 m and becomes zero from 315 m. In the first 50 m, line B is characterized by seaward-dipping reflections with inclinations ranging from 10 to 13°. Between 50 and 250 m, the profile shows sigmoidal reflections, still dipping seaward, with inclinations ranging from 3 to 6° in the lower part and from 6 to 8.5° in the upper part. A high-amplitude horizontal reflection appears at the bottom of the ridge, between 175 and 315 m, at an elevation of 3 m. In the landward most part of the line, the reflections are oblique to sigmoidal. They dip landward with steep inclinations ranging from 13 to 14.5°, and show downlap termination on the high-amplitude reflection previously described.

Line C is a 50 m-long profile that crosses a single ridge of a barrier spit unit of set N5 elongated towards the north and whose mean elevation is 8 m (Fig. 6b). The mean signal penetration depth is 4 m. Line C displays seaward-dipping reflections with an average inclination of 8.5°. These reflections lean on landward-dipping reflections with inclinations of about 6.5°.

Line D is a 250 m-long profile that crosses two barrier sets, N3 at an elevation of 11 m, and N2, at an elevation of 12 m (Fig. 6c). The two barrier sets represent barrier spit units elongated towards the SE. The signal penetration is void on the higher set (N2) and reaches 5 m on the lower set (N3). The internal architecture of this barrier unit is characterized by seaward-dipping reflections with inclinations ranging from 9 to 13.5°.

4.2.3. Lines E-F-G

GPR lines E, F and G are situated on a 2-km long ridge (N4c) oriented NW-SE in alignment with the barrier spit unit described with line D (Fig. 2). The width of the ridge ranges from 20 to 110 m and its mean elevation is 10 m. The maximum signal penetration depth over this ridge is 3 m (Fig. 7).

Line E, shot along the ridge crest, is a 215 m-long profile that shows sub-horizontal and discontinuous reflections (Fig. 7a). At the bottom of the line, a high-amplitude reflection with occasional v-shaped discontinuities is observed at elevations ranging from 7 to 9 m. Line F is a 145 m-long profile that crosses the tidal flat and the ridge at the level of line E start (Fig. 7b). At that point the thickness of the ridge, over the high-amplitude reflection, is the highest (c. 2.5 m). The elevation of the tidal flat decreases from 9 m landward to 7.5 m seaward. The beginning (seaward side) of line F, until 90 m, is characterized by seaward-dipping reflections with inclinations of around 8–11.5°. The landward side of line F displays sub-horizontal to landward-dipping reflections that downlap on the high-amplitude reflection observed on line E. On line F, it shows seaward inclination of 2°.

Line G is a 85 m-long profile, parallel to line F, and located at the level of line E end (Fig. 7c). It also displays seaward-dipping reflections but with gentle inclinations ranging from 7 to 10°, and that downlap the same high-amplitude reflection observed in line E and F, which here has an inclination of 4.5°. On the landward side, reflections are horizontal to sub-horizontal over the high amplitude reflection.

4.2.4. Line H

GPR line H is a 300 m-long cross-shore profile, oriented N-S, located on a beach ridge unit of the sets N4 and N5 (Fig. 2). This beach ridge unit is characterized, from land to sea, by a topographic crest at an elevation of 10 m, a flat area spanning 125 m at an elevation of 9 m, and a second topographic crest at an elevation of 9.5 m, which corresponds to the top of the current beach profile (Fig. 8). However, the actual top of the active beach profile is delimited by a topographic irregularity at an elevation of 6 m. The mean signal penetration depth is 3 m and decreases progressively landward and seaward.

In the first 100 m of line H, a sub-horizontal, high-amplitude reflection is observed at an elevation of 7 m. This reflection plunges eastwards (seaward) with an inclination of 4.5°. The change in slope of this reflection occurs beneath the first crest of the barrier. The reflections above the high-amplitude reflection are sub-horizontal to slightly landward-dipping. From 50 to 300 m, the reflections are mostly seaward-dipping with various angles ranging from 4 to 10°. The first reflection of this seaward package, at 50 m, is clearly erosive on the sub-horizontal reflections observed above the high-amplitude reflection. Locally, it is possible to observe sub-horizontal reflections onlapping the oblique reflections and forming reflection packages dipping steeply seaward. Such packages are particularly well preserved below the most seaward ridge. There, the bottom limit of packages corresponds to the upper part of the modern beach profile. In the final meters, the signal penetration depth decreases to less than 1 m, and the only observable reflections are consistent with the topography of the beach profile.

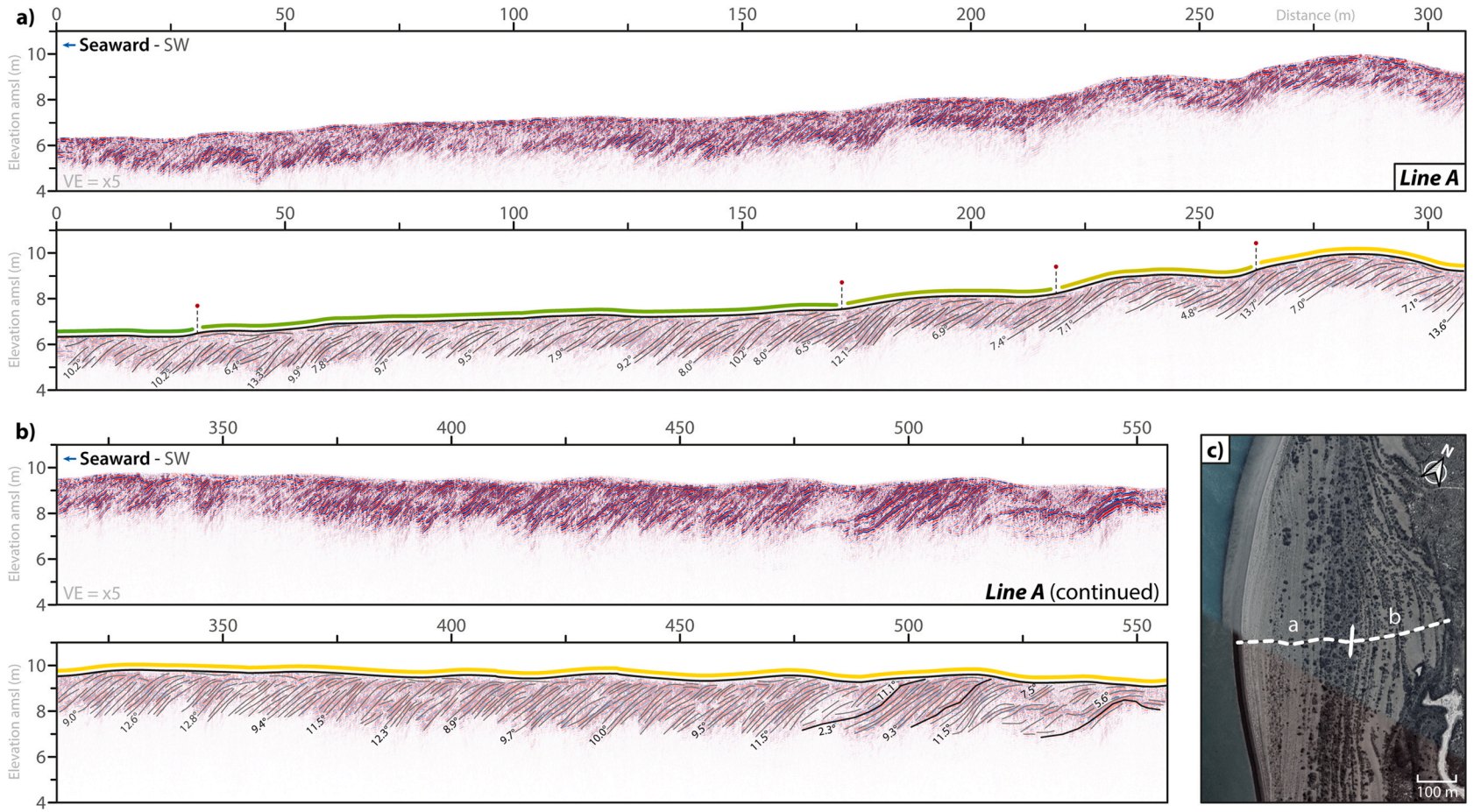

Fig. 5. Interpretation of the GPR line A, situated in the western part of the northern bank (set N4 and N5). (a,b) GPR data and line drawing, (C) Google Earth image with the position of the GPR line. Red dots indicate sub-set boundary from N4 (yellow color) to N5 (green color).

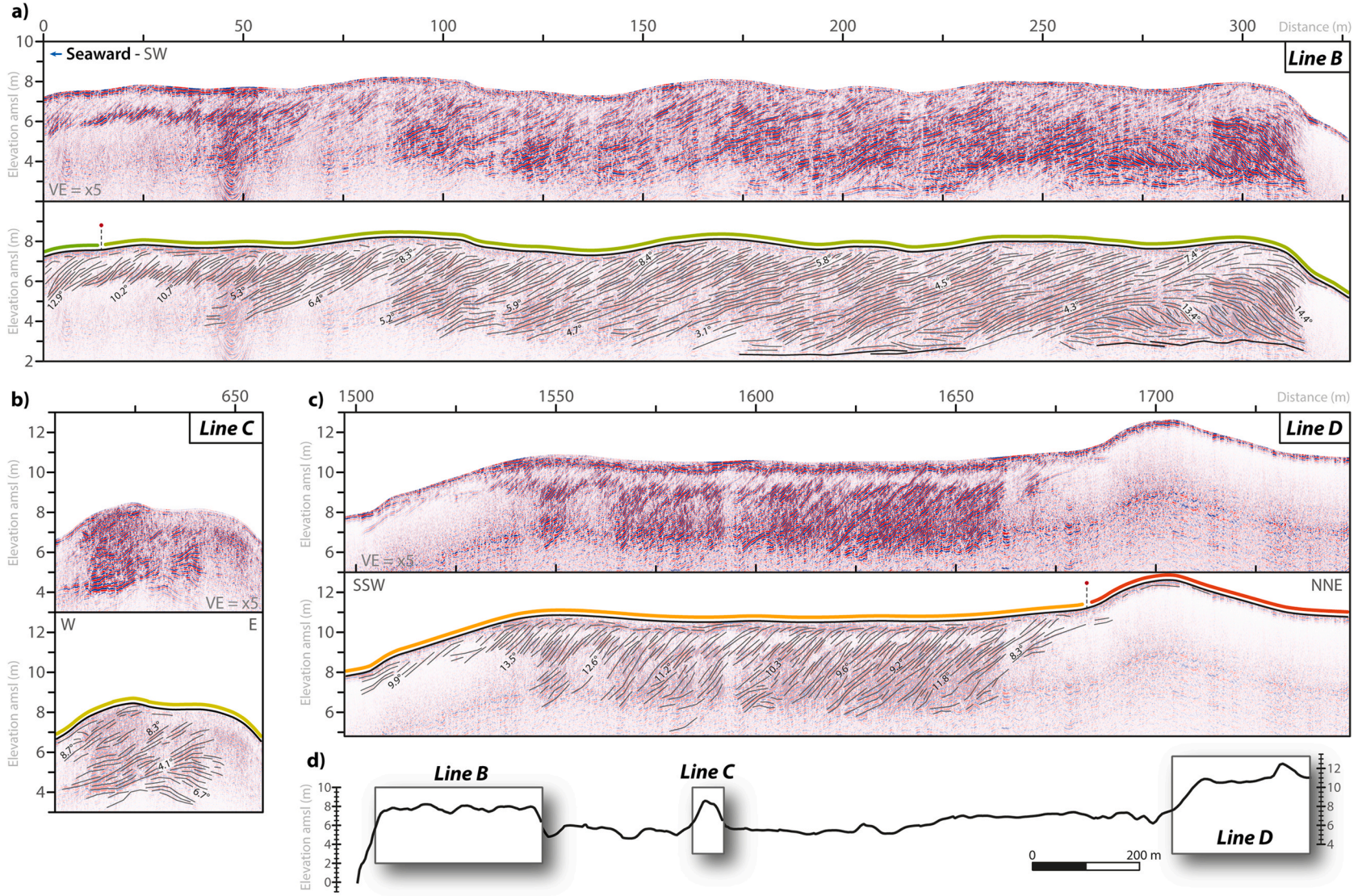

Fig. 6. Interpretation of the GPR lines B, C and D, situated in the central part of the northern bank (sets N2, N3 and N4). (a,b,c) GPR data and line drawing, (d) Topographic line with the position of the GPR lines B,C and D. Red dots indicate sub-set boundary from N2 (red color) to N3 (orange color) to N5 (green color).

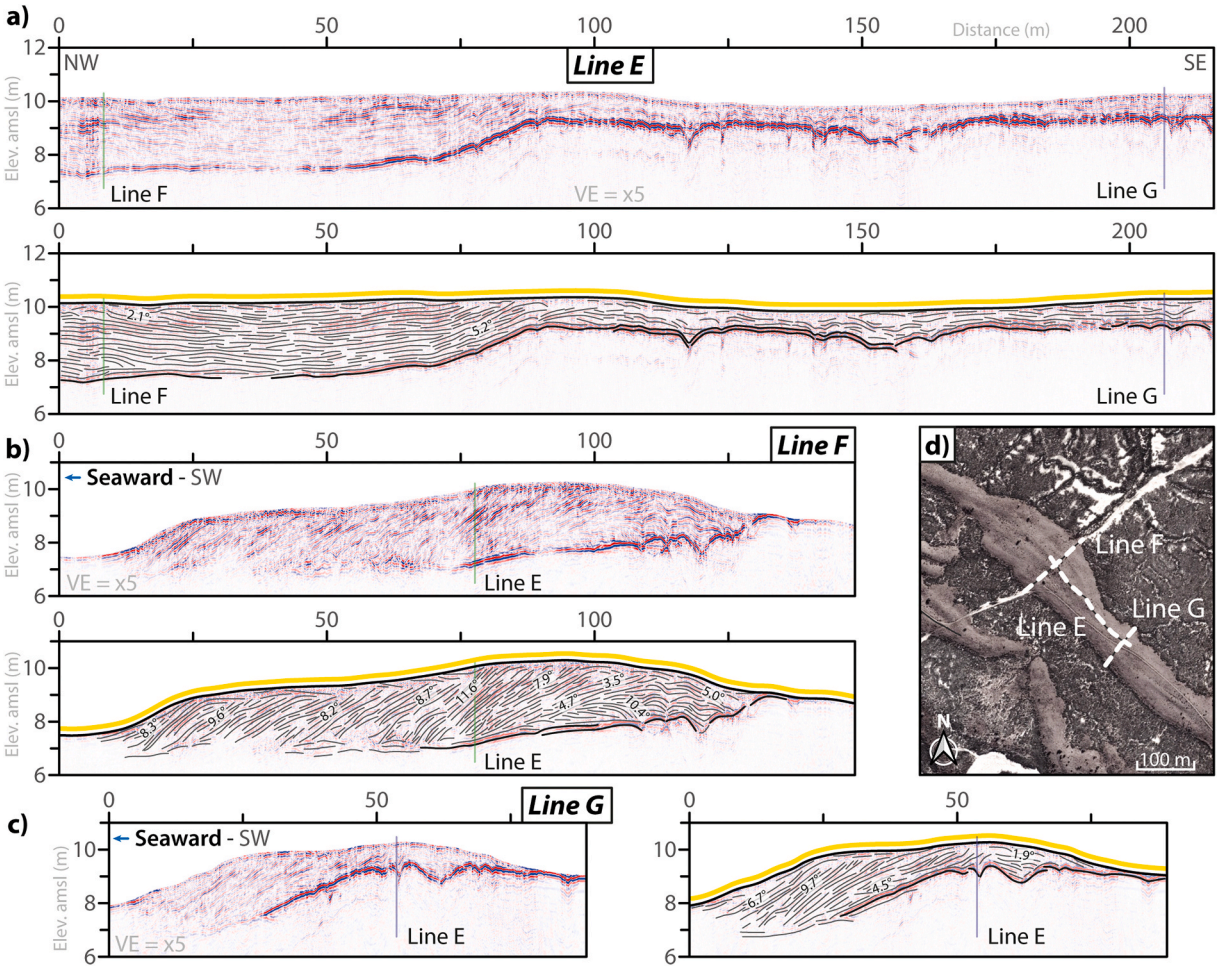

Fig. 7. Interpretation of the GPR lines E, F and G, situated in the central part of the northern bank (set N4). Lines F and G are cross-shore GPR lines that cross perpendicularly the longitudinal line E. (a,b,c) GPR data and drawing lines, (d) Google Earth image with the position of the GPR line.

4.2.5. Lines I-J

GPR lines I and J are both 500 m-long cross-shore profiles intersecting sets S1 and S2 in the southern area (Fig. 2). Line I is oriented NW-SE and faces to the inner estuary and line J is oriented NE-SW and faces to the open sea.

Line I cuts through the barrier spit unit S2d whose elevation ranges from 6 to 8.5 m (Fig. 9a). The mean signal penetration depth is 3 m in the first 200 m and decreases to 2 m under the aeolian dunes that are located landward. In the area of higher penetration, the line is characterized by steep seaward-dipping reflections with inclinations ranging from 9 to 12°. At 50 m, a steeper reflection of more than 16° is followed seaward by a series of gently sloping reflections whose inclinations increase progressively until recovering the average value (Fig. 9c). From 200 to 475 m, the subsurface geometry is divided in two parts: (1) an upper part, above 6 m, where signal intensity is relatively low compared with the lower part, and where only a few sub-horizontal reflections are visible, and (2) a lower part, under 6 m, composed of poorly-organised oblique reflections with inclinations below 6° that are for most of them dipping seaward.

Line J cuts through three inactive barrier units (S1, S2a and S2b), whose elevations decrease seaward from 10.5 to 7 m (Fig. 9b). The highest barrier set S1 corresponds to barrier spit units whereas the lowest barrier set S2 corresponds to beach ridge units (Fig. 2). The mean signal penetration depth is highly variable along the line and ranges from 1 to 4 m. The areas of lower penetration correspond to ridge crests, where the most vegetation is found. At the highest barrier set, above 9 m, the barrier architecture is characterized by sub-horizontal to slightly seaward-dipping reflections with inclinations of less than 4°. The transition between sets S1 and S2 is characterized by sub-horizontal reflections extending from 125 to 175 m. From 175 m to the end of the line, the internal architecture is mostly composed of convex up reflections showing seaward asymmetry, extending from a depth of 4 m to the surface (Fig. 9d). The inclination of the seaward-dipping reflections decreases progressively from 6 to 1° until the topographic crest situated at 430 m under where there is no signal. The reflections situated after the topographic crest displays various inclinations ranging from 2 to 5° and are less organised as the previous one. The transition between the two lowest barrier units, S2a and S2b, shows no major change in the internal architecture.

5. Discussion

5.1. Internal architecture of the barrier units

The architectural elements that characterize the different barriers investigated in the barrier system of the SCCR estuary by GPR can be summarized as follows:

- Most barriers contain GPR reflections which image a dominant mode of construction by progradation. These more or less inclined reflections correspond to beachfaces.
- In the barriers most exposed to ocean waves, beachface reflections show lower inclination in average. Moreover, beachface

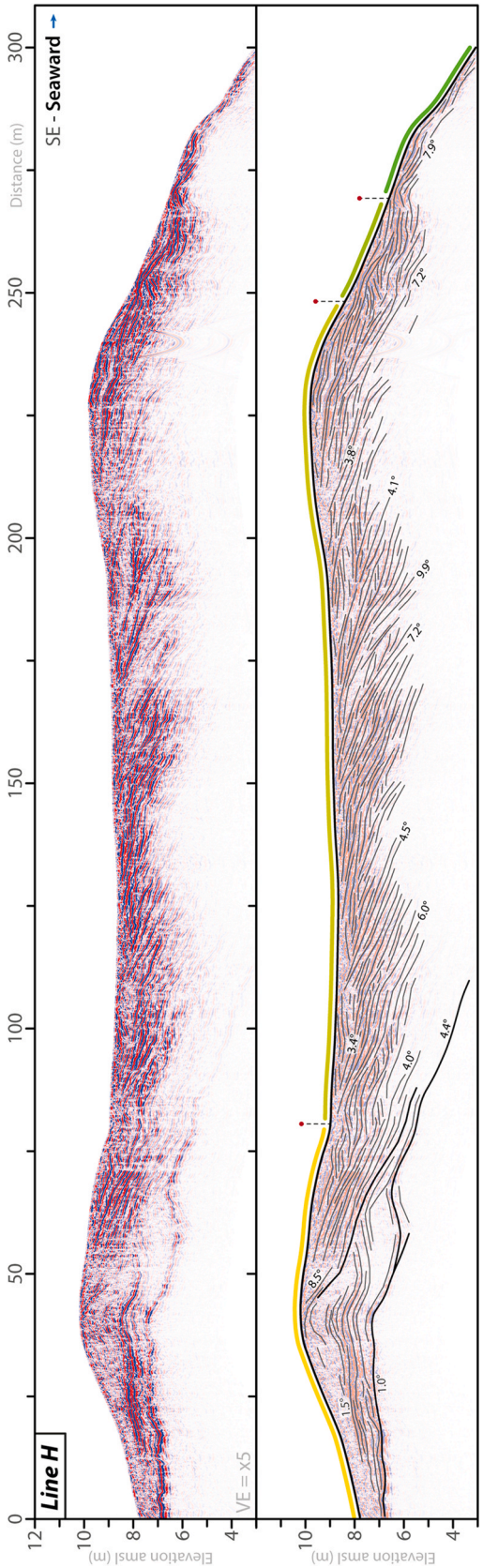

Fig. 8. Interpretation of the GPR line H, situated in the eastern part of the northern bank.

progradational packages contain internal reflections featuring stepped berms (e.g. Figs. 8 and 9d).

- In the northern side, the geometric relationship between the barriers and the associated tidal flat is characterized by landward-dipping reflections at the initial stage of the barrier construction, featuring washover deposits (e.g. Figs. 6a and 7b).
- In the southern side, the prograding beachface packages can display locally very pronounced erosion surfaces, that could be interpreted as cut-and-fill structures (e.g. Fig. 9c).

Our analysis of the system, combining morphological and GPR data provides an overview of the internal architecture patterns that characterize the different types of barriers composing the system (simple ridges, barrier spits and beach ridge plains), and the dominant mode of their behavior (transgressive, regressive or elongation modes). The key control factors are discussed below.

- Simple ridges: their internal architecture is characterized by transgressive geometries (washover) leaning on a topographic step of the tidal flat, followed by a dominant progradational phase. Transgressive patterns have already been observed and described on gravel beaches in southern England, such as in Chesil Beach (Bennett et al., 2009) and Colne Point (Neal et al., 2003), where the same kind of transgressive geometries rely on back-barrier horizontal deposits. On the other side, the combination of transgressive washover and regressive beachface geometries, which commonly characterizes the studied ridges in the SCCR estuary, is not frequently described. An example is provided by Dickson et al. (2009) along the south Canterbury coast in New Zealand, where this configuration is linked to a change in the substrate relief. Although we do not have information on the tidal flat substrate topography, we also believe that simple ridges initiate along steps incised into the underlying flat. The key features in favour of this hypothesis are the abrupt morphology of the basal reflection (Fig. 7), and the alignment of some of the ridges with the paleo-cliffs to the north-west and south-east (e.g. N3a, N4c – Fig. 2).
- Barrier spits: we considered them as transgressive barriers, which develop mainly through elongation but share some similarities with regressive barriers, as progradational sequences can result from their development. This category is largely represented in the SCCR estuary, and on the world's coastlines in general. From a morphological point of view, and when progradation surpasses erosion (i.e., regressive trend), the upstream part of barrier spit is similar to any beach ridge sequence, and may be undifferentiated in some cases (e.g. Engels and Roberts, 2005; Harvey, 2006; Montes et al., 2018). The internal architecture of barrier spits is characterized by steep beach face surfaces, ranging from 9 to 14°, and the absence of well-developed berm deposits. Cut-and-fill structures are another feature that can be observed at the intersection of barrier spits units, but instead of being associated with channel dynamics (e.g. Bristow et al., 2000; Lindhorst et al., 2008), they are associated with the creation of new ridges, as in the initial hypothesis of Davies (1957).
- Beach ridge plains: these progradational morphologies are mainly located in the most exposed areas of the SCCR barrier system. Their internal architecture is composed of low-angle surfaces with angles ranging from 1 to 5°, and berm geometries. As the difference in elevation of the successive ridges is not so important, and as there are no major erosional truncations in their internal architecture, we believe that extreme storm events do not participate significantly to the morphodynamics of these barriers that are rather built by constructional waves. According to Tamura (2012), the previous statement is important to differentiate types of beach ridges, and the development of wave-built barriers with little or no influence from storms seems to be closely related to sea level oscillations. Three main factors can explain why storm impacts are not well-recorded in these beach ridges: (1) extreme events might not be frequent on this

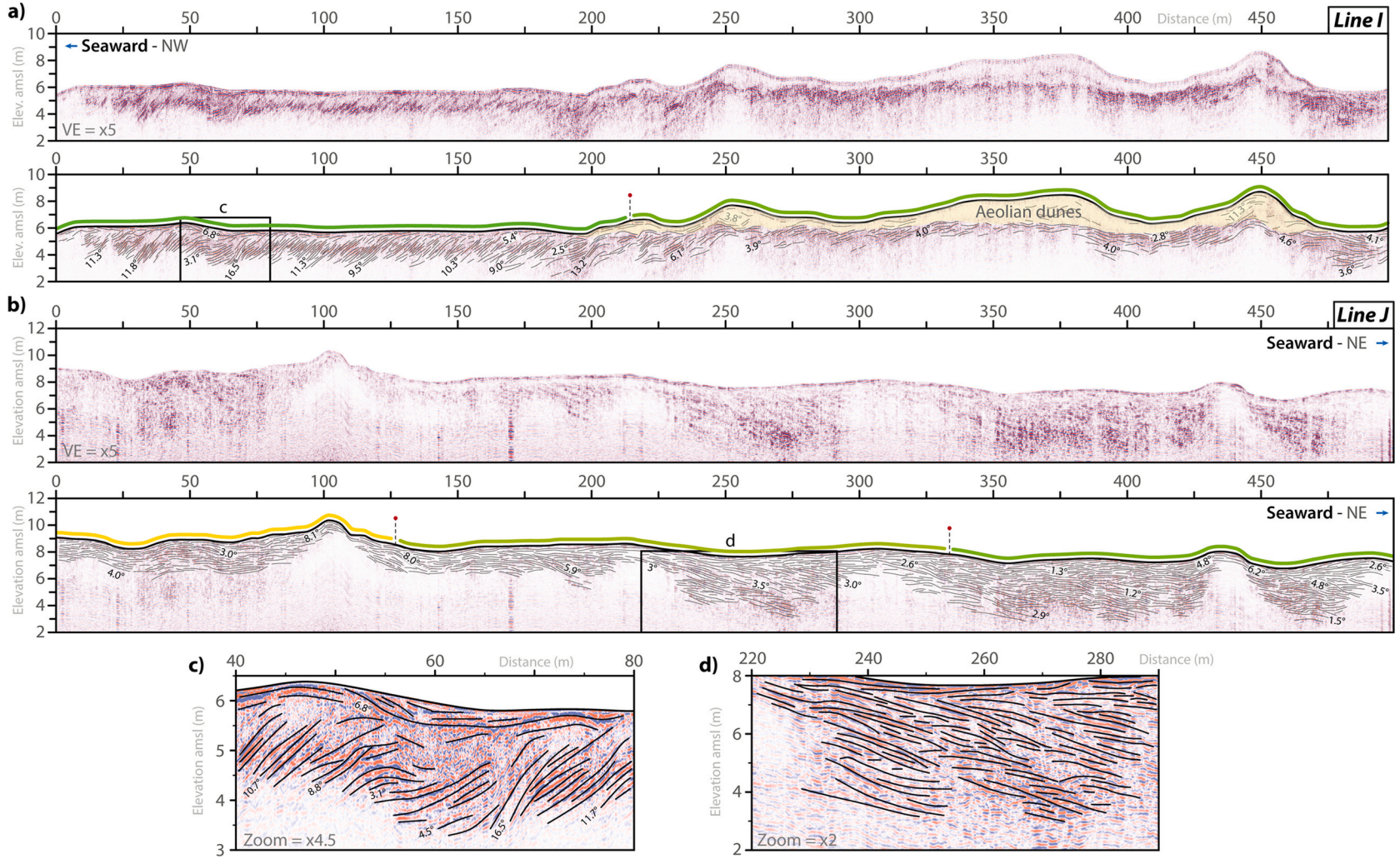

Fig. 9. Interpretation of the GPR lines I and J, situated in the southern bank (sets S1 and S2). (a,b) GPR data and drawing lines, (c) Zoom of the GPR line I, (d) Zoom of the GPR line J. Red dots indicate sub-set boundary from N4 (yellow color) to N5 (green color).

area; (2) coarse-grained barriers have a certain resilience to extreme events by absorbing and reflecting wave energy (Orford and Anthony, 2011; Pollard et al., 2022), and (3) upper beach is only active during spring high tide level, especially on hypertidal coasts.

5.2. Preserved beachface morphologies and wave climate

As each of the barrier morphologies of the SCCR system displays a characteristic internal architecture, we hypothesise that the conditions leading to their formation are somehow preserved. Indeed, the wave conditions, and more specifically the net coastal drift transport, associated with the construction of these morphologies are different. The net sediment transport is assumed to be greater in the case of barrier spits than in the case of beach ridge plains. The main architectural difference between both barriers is the slope of the beach face. The steepness of the beach face is mainly controlled by grain size, with coarser grain-size leading to steeper beaches (McLean and Kirk, 1969; Jennings and Shulmeister, 2002), but it is also controlled by the strength of the littoral drift, with steeper beaches as a result of a stronger littoral drift (Castanho, 1970; Komar, 1971; Sayao and Nairn, 1989). This statement is in accordance with our observations as, despite variable grain-sizes across the system, barrier spits have steeper beach face sequences than beach ridges plains. This potential relationship can be useful to assess the swell's angle of approach, and therefore the barrier exposure.

5.3. How are tidal dynamics recorded within coarse-grained barriers?

The hypertidal regime actually promotes the development of thick gravel beach ridge sequences, and this is the case for the SCCR estuary. GPR data do not allow to image in depth the entire sequences, so that tidal range is difficult to infer from barrier thickness information provided by GPR data. However, GPR data obtained in barrier spit and simple ridge sequences allow evaluating the thicknesses of the upper beachface to 3–5 m. This value does not correspond to the entire tidal range, but rather to the difference in elevation between neap and spring high tide levels. The preservation of berm geometries at different elevations within the upper section (4–5 m) of beach ridge sequences (e.g. Fig. 9d) has already been observed by Montes et al. (2018), and suggests the occurrence of significant water level variations in combination with waves, consistent with hypertidal range. Stepped berms like these are less likely to be preserved when the tidal range is lower due to the constant action of waves on the barrier. The differences between beach ridges and barrier spits, in terms of tidal influence, are mainly attributed to their specific morphodynamics which, in the case of barrier spits, is linked to the development of the platform on which they grow (Allard et al., 2008; Pancrazzi et al., 2022).

The elevation of the barriers, as reported by Bluck (2011), seems to be a better tidal range indicator than the thickness of the gravel sequences as the crest elevation seems to be common to all kind of barriers. In the SCCR system, the crest elevation of the most recent barriers is 6 m a.m.s.l., which means that the thickness of the coastal sequence is similar to the tidal range (i.e. 12 m). The validity of this elevation as a marker is reinforced by the consistency of the sedimentary architecture and the absence of major overtopping structures, especially within barrier spits.

5.4. Late Quaternary evolution of the SCCR coastal barrier system

The results of our geomorphological and internal architecture analyses of the coarse-grained barriers system of the SCCR estuary, combined with data from different authors about regional relative sea level variation allow to propose a schematic evolution model of the mouth of the estuary since the Last Interglacial Maximum (LIM). This evolution can be divided in six main stages (Figs. 10 and 11):

- Stage A: formation of the upper barrier set (N1) on the northern edge of the inlet during MIS 5e (130-115 kyr BP). The orientation of the main barrier spit of the set (N1a) suggests a local seaward littoral drift. Due to the more than 20-km long basin, it is conceivable that prevailing winds, from the same direction as today (i.e. westerlies), would have been capable of generating a littoral drift away from the estuary. The elevation of the upper set (15.5 ± 1 m a.m.s.l) is consistent with the 16 ± 2 m a.m.s.l of some Pleistocene (MIS 5e) beach ridges described further south, at the Rio Gallegos estuary

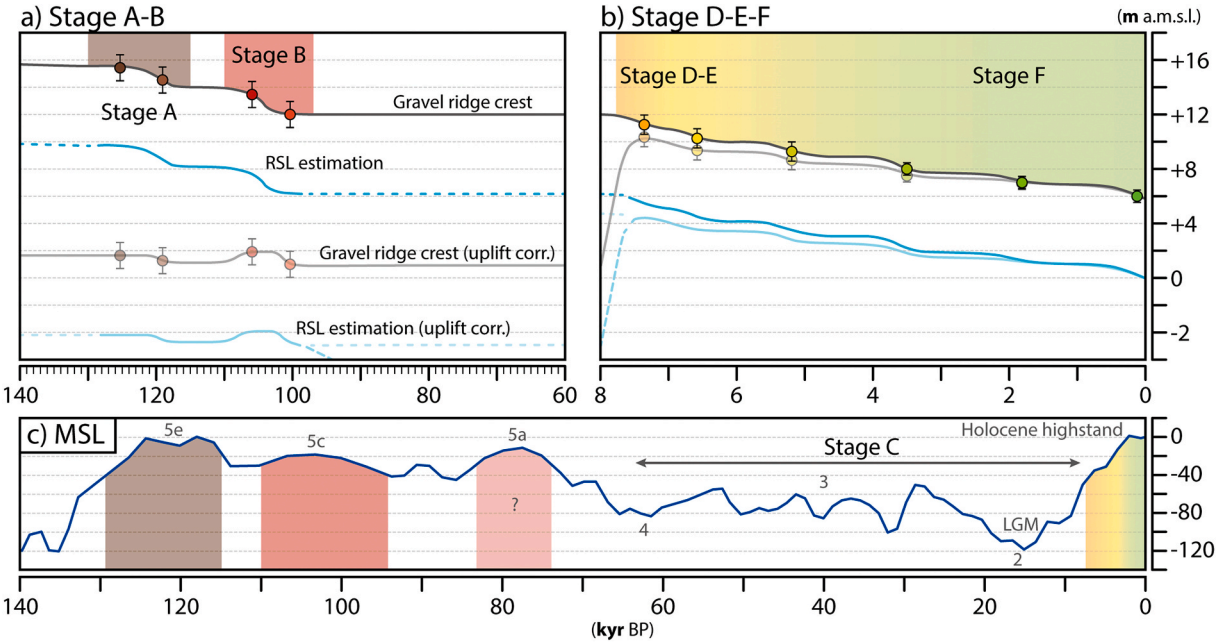

Fig. 10. *Estimated period of development of the SCCR barrier sets and evolution of mean RSL during the late Quaternary in South Patagonia. a) Stages A and B during the last interglacial stage, b) Stages D, E and F during the Holocene, c) Mean sea level (MSL) model from Cocos Ridge (after Lea et al., 2002). According to the current beach profile, the RSL estimation curve (blue color) is placed 6 m (half the tidal range) below the gravel ridge crest curve (black color). The uplift correction in the transparent curves is calculated on the basis of an average uplift rate of 0.*11mm/yr *(Pedoja et al., 2011).*

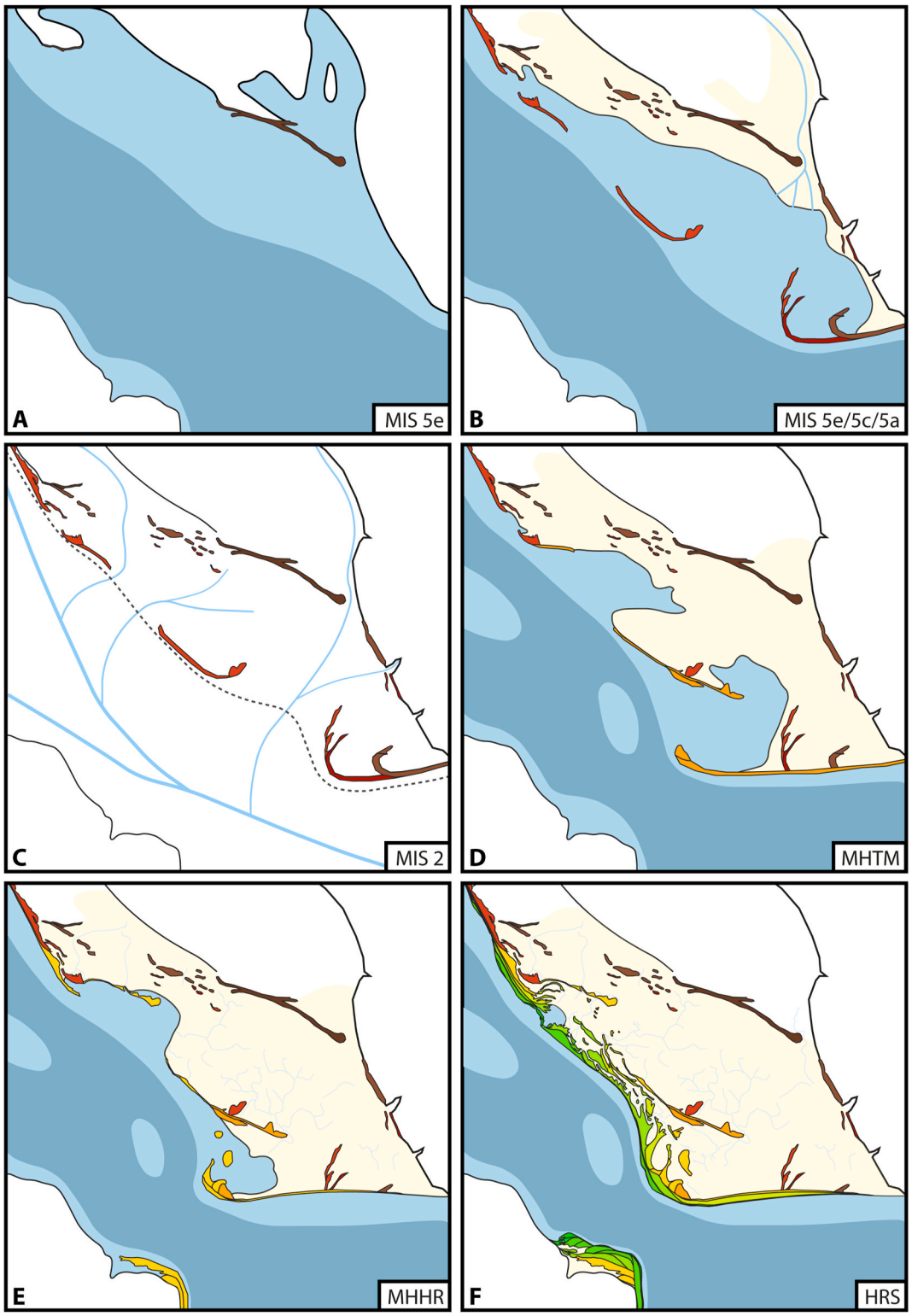

Fig. 11. *Morphological evolution of the SCCR barrier system during the late Quaternary*. According to GPR and elevation data, 5 main stages of evolution are distinguished: A and B are assigned to the last interglacial stage (ca. 120 to 80 kyr BP); C to the Last Glacial Maximum; D and E, to the Maximum Holocene Highstand at c. 7.5 kyr BP (called MHTM: Mid Holocene Transgressive Maximum) and to the following stillstand period until c. 6.5 kyr BP (called MHHR: Mid Holocene Highstand Rework), and E to the Holocene Regressive Stage (HRS) from c. 6.5 kyr BP to present.

(Ercolano, 2010). However, the set is largely above the 12 ± 1 m a.m.s.l of the Pleistocene beach ridges described further north, at Puerto Deseado (Zanchetta et al., 2014). According to Rostami et al. (2000) and Pedoja et al. (2011), the elevation of the Late Pleistocene marine terrace is not well defined in this area with an elevation of 15 ± 4 m a.m.s.l., which is broadly consistent with the elevation of the N1 ridges in the SCCR estuary. The lack of GPR signal can be explained by the presence of pedogenetic iron oxides, which are known to decrease signal penetration (Van Dam et al., 2002; Bristow

and Jol, 2003). These soils can be found all over the Patagonia and they are related to warmer interglacial periods, and more specifically to the MIS 5e stage (Bouza, 2012, 2014).

- Stage B: development of several spits in the northern side of the inlet. The mean elevation of N2 (12 ± 1 m a.m.s.l) is similar to the elevation of another barrier spit unit at the Rio Gallegos estuary, which has been categorised as Holocene deposits (Ercolano, 2010). However, the absence of GPR signal (e.g. Line D – Fig. 6C), as well as the morphological discordance of N2 with the younger barrier sets within the tidal flat suggest that N2 did not develop during the Holocene. The clear separation between N1 and N2 suggests that N2 did not develop during the LIM (MIS 5e) either, but at a slightly more recent stage (i.e. MIS 5c/5a – 100-80 kyr BP, Fig. 10a). This age and elevation would be consistent with the beach ridges observed by Zanchetta et al. (2014) at Puerto Deseado.
- Stage C: intermediate stage corresponding to the Last Glacial Maximum (MIS 2–20 kyr BP). The inlet area is a fluvial environment. Late Pleistocene barrier sets and tidal flat terraces are abandoned, as observed in other coastal areas of Patagonia (e.g. Montes et al., 2020, Tierra del Fuego). No major morpho-sedimentary features for this period have been identified on the GPR data, but the preserved spit morphologies of N1 and N2 sets suggest they were partially eroded by tributary fluvial channels, pointing to a limited barrier reworking (Fig. 10c).
- Stage D: development of a new set of spits in the northern side of the inlet (N3), oriented landward and seaward. The presence of a spit oriented seaward (N3a) proves that the local littoral drift towards the outer estuary observed during stage A is maintained. The good GPR penetration and the elevation of the barrier units (11.2 ± 0.7 m a.m.s.l), consistent with the elevation of the highest Holocene ridges in the region (e.g. Zanchetta et al., 2014), suggest that N3 developed during the transgressive maximum in the Middle Holocene (c. 7.4 kyr BP – Schellmann and Radtke, 2010). The barrier units of N3, predominantly composed of spits, are probably mostly derived from the reworking of the Pleistocene spits. To the east, the growth of the main spit may have reduced the width of the inlet to almost the present width.
- Stage E: development of the first barrier spit units on the southern side of the inlet (S1), and cannibalisation of the main spit of the northern side (N4). Due to their elevation, between 9.5 and 11 m a.m.s.l, these barriers should have also developed during the Holocene. Their transgressive character suggests that these sedimentary bodies were created during the stillstand period following the maximum Holocene highstand (7.4–6.6 kyr cal BP – Schellmann and Radtke, 2010). This stage highlights a change in the coastal hydrodynamics, which favours a northward coastal drift in addition to the main southward coastal drift that led to the development of the barrier units on the northern side of the inlet. Some modifications of the regional hydrodynamics, leading to local reversals of the littoral drift, have been already identified along the South American coast during the late Holocene (e.g. Martin and Suguio, 1992; Isla and Bujalesky, 1995; Isla and Espinosa, 1995), but have not significantly controlled the morphology of the coastal barriers (Codignotto et al., 1990). The hypothesis of the occurrence of a tsunamigenic event during this stage, triggering the development of this barrier set, cannot be ruled out due to the presence of some geomorphological evidence made in Tierra del Fuego (Bujalesky, 2012). However, the presence of a well-developed barrier spit unit on the southern side of the inlet suggests that a more permanent change in the local hydrodynamics has occurred, possibly associated with a modification in the nearshore bathymetry during the Holocene highstand.
- Stage F: final upbuilding of a continuous barrier, and infilling of the back-barrier tidal flats on both sides of the inlet. Although the main sedimentary input is towards the inner estuary, part of the sedimentary input come from the upstream part of the estuarine basin, as shown by the different spits oriented seaward (e.g. N5c – Fig. 2). It is therefore possible to infer that, despite the shrinking of the estuarine basin and the inlet, there has been enough fetch to generate a slight local littoral drift seaward. This stage corresponds to the ultimate Holocene regressive stage, observed in most of the Patagonian coarse-grained barriers (Codignotto et al., 1990; Schellmann and Radtke, 2010; Zanchetta et al., 2014). One to three relative sea level falls have been identified and dated in the coastal barriers from different locations of Patagonia. According to Schellmann and Radtke (2010), the two main relative sea levels falls occurred between 6600 and 6400 cal BP, and between 2300 and 2050 cal BP. The preservation of this regressive sequences is not uniform across the SCCR barrier system. In the northern side of the inlet, the regressive stage is represented by one unit on the most seaward area, two units on the central area, and four units in the most inner estuarine part of the system. In the southern side of the inlet, the regressive stage is represented by three barrier units. The internal architecture at the boundaries of these Late Holocene barrier units shows uniform facies with some slope readjustments, but without any major erosional surface. The increase in the number of preserved units is associated with the fact that the innermost barriers are more protected from erosion of the large oceanic waves than those facing the ocean.

6. Conclusion

This study described a combined analysis of the internal architecture and geomorphology of the coarse-grained coastal barrier system located at the mouth of the hypertidal Santa Cruz – Chico river (SCCR) estuary, in South Patagonia. The data collected allows to find out more about this type of wave-built sedimentary body in a strongly tide-dominated environment. Combined with data on the regional relative sea level (RSL), our data have also permitted to propose a reconstruction of the different stages in the system evolution during the Late Pleistocene and Holocene. The following conclusions can be drawn:

1. The SCCR barrier system is composed of three main barrier types: barrier spits, beach ridge plains and simple ridges. Each barrier type can be identified by its sedimentary architecture and, in particular, by the slope of the beach face. Barrier spits and elongated simple ridges display steep beach face strata with slopes ranging from 9 to 14°, while in beach ridges slopes of beach face deposits are weaker, between 1 and 5°. This stratigraphical differentiation allows linking the sediment record to the strength of the coastal drift, thus informing about the barrier exposure to open sea dynamics.
2. Although located in a hypertidal domain, the tidal signature does not appear clearly in the architecture of the different barrier types. Only the stepped berms preserved in the upper section (4–5 m) of the most exposed beach ridges may reveal the tidal context.
3. The elevation of active (modern) coarse-grained barrier crests located in protected areas, such as spits and ridges more developed into the estuary, can be considered as a valuable proxy of the highest tide level (and thus of the tidal range). For older ridges and spits, this elevation is an estimate of the relative sea level.
4. Five main barrier sets with elevations ranging from 16.5 to 6 m a.m.s.l. are identified in the SCCR barrier system. All the barrier sets are present in the northern side of the inlet, but only the lowest ones are found in the southern side. According to their elevation and regional data, the approximate period of development of each barrier set has been proposed. The two highest sets are associated to the Last Interglacial Maximum (MIS 5e), although the lowest of the two could be associated with the MIS 5c or MIS 5a stages. The three lowest sets are Holocene, among which the two highest mark (3) the Holocene transgression maximum around 7.5 kyr BP, and (4) the Holocene highstand rework. The lowermost set formed during (5) the Holocene regressive period. This last stage of development highlights a

gradual decrease in the RSL resulting in four sub-stages, stepped between 10 and 6 m a.m.s.l.

5. The morphological evolution model proposed in line with the five stages described previously needs to be consolidated with absolute dating.

CRediT authorship contribution statement

Léo Pancrazzi: Writing – original draft, Visualization, Investigation, Data curation, Conceptualization. **Bernadette Tessier:** Writing – original draft, Supervision, Project administration, Investigation, Funding acquisition, Conceptualization. **Pierre Weill:** Writing – original draft, Supervision, Conceptualization. **Dominique Mouazé:** Writing – review & editing, Supervision, Conceptualization. **José Ignacio Cuitiño:** Writing – review & editing, Investigation. **Jean-Yves Reynaud:** Writing – review & editing, Investigation. **Maria Duperron:** Writing – review & editing, Investigation. **Roberto Adrián Scasso:** Writing – review & editing, Investigation. **Alejandro Montes:** Writing – review & editing.

Declaration of competing interest

The authors declare that they have no known competing financial interests or personal relationships that could have appeared to influence the work reported in this paper.

Data availability

Data will be made available on request.

Acknowledgements

This study is based on the doctoral work of L. Pancrazzi, funded by the French Ministry of Higher Education, Research and Innovation, and financially supported by the program ECOS-Sud (CNRS-INSU) and the "Agence de l'Eau Artois-Picardie". The first author acknowledges Kevin Pedoja (University of Caen) for the discussions on regional tectonics.

Appendix A. Supplementary data

Supplementary data to this article can be found online at https://doi.org/10.1016/j.jsames.2024.105073.

References

Allard, J., Bertin, X., Chaumillon, E., Pouget, F., 2008. Sand spit rhythmic development: a potential record of wave climate variations? Arçay Spit, western coast of France. Mar. Geol. 253 (3–4), 107–131. https://doi.org/10.1016/j.margeo.2008.05.009.

Archer, A.W., 2013. World's highest tides: hypertidal coastal systems in North America, South America and Europe. Sediment. Geol. 284, 1–25. https://doi.org/10.1016/j.sedgeo.2012.12.007.

Bennett, M.R., Cassidy, N.J., Pile, J., 2009. Internal structure of a barrier beach as revealed by ground penetrating radar (GPR): Chesil beach, UK. Geomorphology 104 (3–4), 218–229. https://doi.org/10.1016/j.geomorph.2008.08.015.

Bertels, A., 1970. Sobre el "Piso Patagoniano" y la representación de la época del Oligoceno en Patagonia Austral, República Argentina. Rev. Asoc. Geol. Argent. 25 (4), 495–501.

Billy, J., Robin, N., Hein, C.J., Certain, R., FitzGerald, D.M., 2015. Insight into the late Holocene sea-level changes in the NW Atlantic from a paraglacial beach-ridge plain south of Newfoundland. Geomorphology 248, 134–146. https://doi.org/10.1016/j.geomorph.2015.07.033.

Bindelli, L., Kazimierski, L., Re, M., 2020. Evaluación del potential energético de las corrientes de marea en estuarios patagónicos mediante modelación numérica: Modelos numéricos y potential energético. Technical report. Instituto Nacional del Agua, Buenos Aires, Argentina, p. 91.

Bluck, B.J., 2011. Structure of gravel beaches and their relationship to tidal range. Sedimentology 58 (4), 994–1006. https://doi.org/10.1111/j.1365-3091.2010.01192.x.

Bouza, P.J., 2012. Génesis de las acumulaciones de carbonatos en Aridisoles Nordpatagónicos: su significado paleopedológico. Rev. Asoc. Geol. Argent. 69 (2), 0-0.

Bouza, P.J., 2014. Paleosuelos en Cordones litorales de la formación Caleta Valdés, pleistoceno superior, noreste de Chubut. Rev. Asoc. Geol. Argent. 71 (1), 1–10.

Bristow, C.S., Chroston, P.N., Bailey, S.D., 2000. The structure and development of foredunes on a locally prograding coast: insights from ground-penetrating radar surveys, Norfolk, UK. Sedimentology 47 (5), 923–944. https://doi.org/10.1046/j.1365-3091.2000.00330.x.

Bristow, C.S., Jol, H.M., 2003. An introduction to ground penetrating radar (GPR) in sediments. Geological Society, London, Special Publications 211 (1), 1–7. https://doi.org/10.1144/GSL.SP.2001.211.01.01.

Brooke, B.P., Huang, Z., Nicholas, W.A., Oliver, T.S., Tamura, T., Woodroffe, C.D., Nichol, S.L., 2019. Relative sea-level records preserved in Holocene beach-ridge strandplains–An example from tropical northeastern Australia. Mar. Geol. 411, 107–118. https://doi.org/10.1016/j.margeo.2019.02.005.

Bujalesky, G.G., 2007. Coastal geomorphology and evolution of Tierra del Fuego (Southern Argentina). Geol. Acta: an international earth science journal 5 (4), 337–362.

Bujalesky, G.G., 2012. Tsunami overtopping fan and erosive scarps at Atlantic coast of Tierra del Fuego. J. Coast Res. 28 (2), 442–456. https://doi.org/10.2112/JCOASTRES-D-11-00037.1.

Castanho, J., 1970. Influence of grain size on littoral drift. Coast Eng. 1970, 891–898. https://doi.org/10.1061/9780872620285.056.

Codignotto, J.O., Marcomini, S.C., Santillana, S.N., 1988. Terrazas marinas entre Puerto Deseado y Bahía Bustamante, Santa Cruz, Chubut. Rev. Asoc. Geol. Argent. 43 (1), 43–50.

Codignotto, J.O., Cesari, O., Beros, C.A., 1990. Morfocronología secuencial evolutiva holocena en Bahía Solano, Chubut. Rev. Asoc. Geol. Argent. 45 (3–4), 205–212.

Codignotto, J.O., Kokot, R.R., Marcomini, S.C., 1992. Neotectonism and sea-level changes in the coastal zone of Argentina. J. Coast Res. 125–133. https://www.jstor.org/stable/4297958.

Dalrymple, R.W., Mackay, D.A., Ichaso, A.A., Choi, K.S., 2012. Processes, morphodynamics, and facies of tide-dominated estuaries. Principles of tidal sedimentology 79–107. https://doi.org/10.1007/978-94-007-0123-6_5.

Davies, J.L., 1957. The importance of cut and fill in the development of sand beach ridges. Aust. J. Sci. 20, 105.

Darwin, C., 1846. Geological Observations on South America. Being the Third Part of the Geology of the Voyage of the Beagle, under the Command of Capt. Fitzroy, R.N. During the Years 1832 to 1836. Smith Elder and Co, London.

Dickson, M.E., Bristow, C.S., Hicks, D.M., Jol, H., Stapleton, J., Todd, D., 2009. Beach volume on an eroding sand–gravel coast determined using ground penetrating radar. J. Coast Res. 25 (5), 1149–1159. https://doi.org/10.2112/08-1137.1.

Elias, E.P., Hansen, J.E., 2013. Understanding processes controlling sediment transports at the mouth of a highly energetic inlet system (San Francisco Bay, CA). Mar. Geol. 345, 207–220. https://doi.org/10.1016/j.margeo.2012.07.003.

Engels, S., Roberts, M.C., 2005. The architecture of prograding sandy-gravel beach ridges formed during the last Holocene highstand: southwestern British Columbia, Canada. J. Sediment. Res. 75 (6), 1052–1064. https://doi.org/10.2110/jsr.2005.081.

Ercolano, B., 2010. Evolución de la costa comprendida entre el río Gallegos y Chorrillo de los Frailes. Facultad de Ciencias Exactas y Naturales, Universidad de, Buenos Aires, Argentina, p. 243. Ph.D. Thesis.

Ezcurra & Schmidt S.A. (ESSA), 2017. Modelación hydrodinamica, dispersión y transporte de sédimentos. Estudio de Campo de Apoyo a la Modelación. Informe de campo, Estuario del Rio Santa Cruz, Provincia de Santa Cruz, p. 33.

Feruglio, E., 1950. Descripción Geológica de la Patagonia. Dirección General de Y.P.F., Buenos Aires, vol. 3, p. 431.

Fruergaard, M., Tessier, B., Poirier, C., Mouazé, D., Weill, P., Noël, S., 2020. Depositional controls on a hypertidal barrier-spit system architecture and evolution, Pointe du Banc spit, north-western France. Sedimentology 67 (1), 502–533. https://doi.org/10.1111/sed.12652.

Harvey, N., 2006. Holocene coastal evolution: barriers, beach ridges, and tidal flats of South Australia. J. Coast Res. 22 (1), 90–99. https://doi.org/10.2112/05A-0008.1.

Iantanos, N., 2004. Dinámica sedimentaria de la Río de Puerto Deseado, Provincia de Santa Cruz. Ph.D. Thesis. Universidad de la Patagonia San Juan Bosco, FCN, Comodoro Rivadavia, p. 172p.

Isla, F.I., Bujalesky, G.G., 1995. Tendencias evolutivas y disponibilidad de sedimento en la interpretación de formas costeras: Casos de estudio de la costa argentina. Revista de la Asociación Argentina de Sedimentología 2 (1–2), 75–89.

Isla, F.I., Bujalesky, G.G., 2000. Cannibalisation of Holocene gravel beach-ridge plains, northern Tierra del Fuego, Argentina. Mar. Geol. 170 (1–2), 105–122. https://doi.org/10.1016/S0025-3227(00)00069-4.

Isla, F.I., Bujalesky, G.G., 2008. Coastal geology and morphology of Patagonia and the fuegian archipelago. Dev. Quat. Sci. 11, 227–239. https://doi.org/10.1016/S1571-0866(07)10010-5.

Isla, F.I., Espinosa, M.A., 1995. Coastal environmental changes associated with Holocene sea-level fluctuation: southeastern Buenos Aires, Argentina. Quat. Int. 26, 55–60. https://doi.org/10.1016/1040-6182(94)00046-8.

Isla, F., Iantanos, N., Estrada, E., 2004. Dinámica submareal y condiciones ambientales de la ría Deseado, Santa Cruz. Rev. Asoc. Geol. Argent. 59 (3), 367–375.

Jennings, R., Shulmeister, J., 2002. A field based classification scheme for gravel beaches. Mar. Geol. 186 (3–4), 211–228. https://doi.org/10.1016/S0025-3227(02)00314-6.

Kokot, R.R., 1999. Cambio climático y evolución costera en Argentina. Facultad de Ciencias Exactas y Naturales, Universidad de Buenos Aires, Argentina 254. Ph.D. Thesis.

Kokot, R.R., Monti, A.A., Codignotto, J.O., 2005. Morphology and short-term changes of the caleta valdés barrier spit, Argentina. J. Coast Res. 21 (5), 1021–1030. https://doi.org/10.2112/03-703A.1.

Kokot, R.R., 2010. Spit as indictors of waves provenance in the coast of Argentina. Rev. Asoc. Geol. Argent. 67 (1), 19–26.

Komar, P.D., 1971. The mechanics of sand transport on beaches. J. Geophys. Res. 76 (3), 713–721. https://doi.org/10.1029/JC076i003p00713.
Lea, D.W., Martin, P.A., Pak, D.K., Spero, H.J., 2002. Reconstructing a 350 ky history of sea level using planktonic Mg/Ca and oxygen isotope records from a Cocos Ridge core. Quat. Sci. Rev. 21 (1–3), 283–293. https://doi.org/10.1016/S0277-3791(01)00081-6.
Levoy, F., Anthony, E.J., Monfort, O., Larsonneur, C., 2000. The morphodynamics of megatidal beaches in Normandy, France. Mar. Geol. 171 (1–4), 39–59. https://doi.org/10.1016/S0025-3227(00)00110-9.
Lindhorst, S., Betzler, C., Hass, H.C., 2008. The sedimentary architecture of a Holocene barrier spit (Sylt, German Bight): swash-bar accretion and storm erosion. Sediment. Geol. 206 (1–4), 1–16. https://doi.org/10.1016/j.sedgeo.2008.02.008.
Martin, L., Suguio, K., 1992. Variation of coastal dynamics during the last 7000 years recorded in beach-ridge plains associated with river mouths: example from the central Brazilian coast. Palaeogeogr. Palaeoclimatol. Palaeoecol. 99 (1–2), 119–140. https://doi.org/10.1016/0031-0182(92)90010-3.
McLean, R.F., Kirk, R.M., 1969. Relationships between grain size, size-sorting, and foreshore slope on mixed sand-shingle beaches. N. Z. J. Geol. Geophys. 12 (1), 138–155. https://doi.org/10.1080/00288306.1969.10420231.
Montes, A., Bujalesky, G.G., Paredes, J.M., 2018. Geomorphology and internal architecture of Holocene sandy-gravel beach ridge plain and barrier spits at Río Chico area, Tierra del Fuego, Argentina. J. S. Am. Earth Sci. 84, 172–183. https://doi.org/10.1016/j.jsames.2018.03.012.
Montes, A., Santiago, F., Salemme, M., López, R., 2020. Late Pleistocene and Holocene geomorphologic evolution of Laguna Las Vueltas area, Tierra del Fuego (Argentina). Andean Geol. 47 (1), 61–76. https://doi.org/10.5027/andgeoV47n1-3219.
Montreuil, A.L., Levoy, F., Bretel, P., Anthony, E.J., 2014. Morphological diversity and complex sediment recirculation on the ebb delta of a macrotidal inlet (Normandy, France): a multiple LiDAR dataset approach. Geomorphology 219, 114–125. https://doi.org/10.1016/j.geomorph.2014.05.008.
Neal, A., Roberts, C.L., 2000. Applications of ground-penetrating radar (GPR) to sedimentological, geomorphological and geoarchaeological studies in coastal environments. Geological Society, London, Special Publications 175 (1), 139–171. https://doi.org/10.1144/GSL.SP.2000.175.01.12.
Neal, A., Richards, J., Pye, K., 2003. Sedimentology of coarse-clastic beach-ridge deposits, Essex, southeast England. Sediment. Geol. 162 (3–4), 167–198. https://doi.org/10.1016/S0037-0738(03)00136-2.
Nielsen, L., Bendixen, M., Kroon, A., Hede, M.U., Clemmensen, L.B., Weβling, R., Elberling, B., 2017. Sea-level proxies in Holocene raised beach ridge deposits (Greenland) revealed by ground-penetrating radar. Sci. Rep. 7 (1), 46460 https://doi.org/10.1038/srep46460.
Nunes, J.C.R., Puhl, E., Aliotta, S., Toldo Jr, E.E., Schffer, P.N.M., Fick, C., Lima-Filho, F. P., Silveira dos Santos, G., Barros, C.A., Secco da Silva, F.R., Schenk, C.V., 2023. Beach ridge sequence evolution of punta verde, northern coast of the san matías gulf, Argentina. J. S. Am. Earth Sci., 104704 https://doi.org/10.1016/j.jsames.2023.104704.
Orford, J.D., Anthony, E.J., 2011. Extreme events and the morphodynamics of gravel-dominated coastal barriers: strengthening uncertain ground. Mar. Geol. 290 (1–4), 41–45. https://doi.org/10.1016/j.margeo.2011.10.005.
Orford, J.D., Carter, R.W., Jennings, S.C., 1991. Coarse clastic barrier environments: evolution and implications for Quaternary sea level interpretation. Quat. Int. 9, 87–104. https://doi.org/10.1016/1040-6182(91)90068-Y.
Otvos, E.G., 2000. Beach ridges—definitions and significance. Geomorphology 32 (1–2), 83–108. https://doi.org/10.1016/S0169-555X(99)00075-6.
Pancrazzi, L., Weill, P., Tessier, B., Le Bot, S., Benoit, L., 2022. Morphostratigraphy of an active mixed sand–gravel barrier spit (Baie de Somme, Northern France). Sedimentology 69 (7), 2753–2778. https://doi.org/10.1111/sed.13018.
Pappalardo, M., Aguirre, M., Bini, M., Consoloni, I., Fucks, E., Hellstrom, J., Isola, I., Ribolini, A., Zanchetta, G., 2015. Coastal landscape evolution and sea-level change: a case study from Central Patagonia (Argentina). Zeitschrift Fur Geomorphologie 59 (2), 145–172. https://doi.org/10.1127/0372-8854/2014/0142.
Parras, A., Griffin, M., 2009. Darwins great patagonian tertiary formation at the mouth of the río Santa Cruz: a reappraisal. Rev. Asoc. Geol. Argent. 64 (1), 70–82.
Pasquini, A.I., Depetris, P.J., 2011. Southern patagonia's Perito Moreno glacier, lake argentino, and Santa Cruz river hydrological system: an overview. J. Hydrol. 405 (1–2), 48–56. https://doi.org/10.1016/j.jhydrol.2011.05.009.
Pedoja, K., Regard, V., Husson, L., Martinod, J., Guillaume, B., Fucks, E., Maximiliano, I., Weill, P., 2011. Uplift of Quaternary shorelines in eastern Patagonia: Darwin revisited. Geomorphology 127 (3–4), 121–142. https://doi.org/10.1016/j.geomorph.2010.08.003.
Piccolo, M., Perillo, G.M., 1999. The Argentina estuaries: a review. Estuaries of South America 101–132. https://doi.org/10.1007/978-3-642-60131-6_6.
Plattner, A.M., 2020. GPRPy: open-source ground-penetrating radar processing and visualization software. Lead. Edge 39 (5), 332–337. https://doi.org/10.1190/tle39050332.1.
Pollard, J.A., Christie, E.K., Spencer, T., Brooks, S.M., 2022. Gravel barrier resilience to future sea level rise and storms. Mar. Geol. 444, 106709 https://doi.org/10.1016/j.margeo.2021.106709.
Robin, N., Levoy, F., Monfort, O., 2009. Short term morphodynamics of an intertidal bar on megatidal ebb delta. Mar. Geol. 260 (1–4), 102–120. https://doi.org/10.1016/j.margeo.2009.02.006.
Rostami, K., Peltier, W.R., Mangini, A., 2000. Quaternary marine terraces, sea-level changes and uplift history of Patagonia, Argentina: comparisons with predictions of the ICE-4G (VM2) model of the global process of glacial isostatic adjustment. Quat. Sci. Rev. 19 (14–15), 1495–1525. https://doi.org/10.1016/S0277-3791(00)00075-5.
Sanjaume, E., Tolgensbakk, J., 2009. Beach ridges from the Varanger Peninsula (Arctic Norwegian coast): characteristics and significance. Geomorphology 104 (1–2), 82–92. https://doi.org/10.1016/j.geomorph.2008.05.029.
Sayao, O.J., Nairn, R.B., 1989. Physical modelling of beach erosion and littoral drift. Coast Eng. 1988, 1818–1832. https://doi.org/10.1061/9780872626874.135.
Schellmann, G., 1998. Jungkanozoische landschaftsgeschichte patagoniens (argentien). Essener Geographische Arbeiten 29, 216p. Essen.
Schellmann, G., Radtke, U., 2000. ESR dating stratigraphically well-constrained marine terraces along the Patagonian Atlantic coast (Argentina). Quat. Int. 68, 261–273. https://doi.org/10.1016/S1040-6182(00)00049-5.
Schellmann, G., Radtke, U., 2003. Coastal terraces and Holocene sea-level changes along the Patagonian Atlantic coast. J. Coast Res. 983–996. https://www.jstor.org/stable/4299242.
Schellmann, G., Radtke, U., 2010. Timing and magnitude of Holocene sea-level changes along the middle and south Patagonian Atlantic coast derived from beach ridge systems, littoral terraces and valley-mouth terraces. Earth Sci. Rev. 103 (1–2), 1–30. https://doi.org/10.1016/j.earscirev.2010.06.003.
Tamura, T., 2012. Beach ridges and prograded beach deposits as palaeoenvironment records. Earth Sci. Rev. 114 (3–4), 279–297. https://doi.org/10.1016/j.earscirev.2012.06.004.
Tessier, B., Reynaud, J.Y., Cuitiño, J.I., Scasso, R.A., Pancrazzi, L., Duperron, M., Weill, P., Bout-Roumazeilles, V., Armynot du Chatelet, E., Kuinkel, A., Lortie, T., Dezilieau, L., 2024. The Hypertidal Santa Cruz – Chico River Estuary (South Patagonia, Argentina): a Hybrid Ria-type System under Extreme Tides, Arid Climate and Active Uplift. Sedimentary Geology (in press).
Van Dam, R.L., Schlager, W., Dekkers, M.J., Huisman, J.A., 2002. Iron oxides as a cause of GPR reflections. Geophysics 67 (2), 536–545. https://doi.org/10.1190/1.1468614.
Zanchetta, G., Bini, M., Isola, I., Pappalardo, M., Ribolini, A., Consoloni, I., Boretto, G., Fucks, E., Ragaini, L., Terrasi, F., 2014. Middle-to late-Holocene relative sea-level changes at Puerto Deseado (Patagonia, Argentina). Holocene 24 (3), 307–317. https://doi.org/10.1177/0959683613518589.